Monografías de la Real Academia de Ciencias de Zaragoza **31**, 199–216, (2009).

Numerical simulation of flood waves induced by landslides

A. Serrano-Pacheco, J. Murillo, P. García-Navarro and P. Brufau

Fluid Mechanics. CPS. University of Zaragoza

50018 Zaragoza, Spain

Abstract

The objective of the work is to design and test a numerical approach able to deal with a class of phenomena quite important for the dam safety, as are the floods induced by landslides. The physical phenomena involved are described assuming that the fluid flow is composed of two layers of incompressible immiscible fluids, a lower heavily concentrated layer of mud flow and an upper layer of clean water. The movement of both layers is governed by a hydrostatic pressure model, based on the two-dimensional shallow water equations. A Bingham fluid model characterizes the landslide movement of the lower layer. An explicit first order in space and time upwind finite volume scheme is used to discretize the system of equations, by means of the Roe's approximate Riemann solver. A special treatment of the source terms arising from the stratification of the layers and the viscous model is required to satisfy exact conservation of the variables involved in equilibrium conditions. The results indicate that the numerical scheme computes the landslide and flooding advance accurately. The numerical scheme was applied to the Santa Liestra dam project on the Esera river (Spain) as a real size practical case, to estimate the impacts of the possible landslides could produce in the zone of the project.

1 Introduction

Dams are usually built in valleys where active erosion is present, and some are in active earthquake areas. Therefore, reservoirs can be vulnerable to landslides activated by earthquakes or by heavy rains and they could generate large waves that can produce flooding over banks or overtopping the dam crest.

As dam safety is a significant issue in dam engineering, studies of these natural accidents and their consequences must be considered in the project phase of a dam and regular operation stages, especially when the construction site is placed in a high risk

seismic activity zone, or when the geological study of the banks indicates the existence of a potential landslide area. The study of these phenomena, including slope failures, the generation of waves and their impacts on the dam should be integrated.

Studies of natural landslides that occur in dam reservoirs show that they were induced mainly by earthquakes or heavy rains. Several ways of landslides classification could be used: sliding mass can be initially non submerged, partially or completely submerged; the material can be more or less compact or dense, granular or fine (rock and soil, snow); the sliding mass volume could be variable from small to great volumes; sliding mass velocity at the moment of the impact is dependent on the balance of forces/moments, which are influenced by the dynamic properties of soil, by the soil brittleness and by topographic effects; the size or volume, and the reservoir depth.

Experimental studies of impulse waves generated by landslides composed by granular rockslide were presented in [5], and other authors like [4].

The Santa Liestra reservoir has been proposed to regulate 81.9 Hm^3 at the upper part of the Esera river, in the Spanish Pyrenees. There was a controversy due the risk associated with potential landslides in the nearby mountains forming the banks of the future reservoir. A study of the waves generated by landslide is in [10]. In this study, they analyzed the effect of the landslide could produce in the zone of the Santa Liestra dam project, with one-dimensional model. The present work is a more detailed study of the hypothetical flood waves that could be triggered by the reservoir's bank failure.

2 Mathematical Model

The main assumptions of the mathematical model are:

- The physical phenomena involved are described assuming that the fluid flow is composed of two layers of incompressible immiscible fluids.
- The movement of both layers is governed by a hydrostatic pressure model, based on the two-dimensional shallow water equations.
- An explicit first order in space and time upwind finite volume scheme is used to discretize the system of equations (Roe's approximate Riemann solver).

A sketch of the model is shown in figure 1. The water flow, in some circumstances, can be modeled according to the shallow water equations (see [8]). The two dimension shallow water equations can be obtained by depth-averaging the Navier-Stokes equations, leading to:

$$\frac{\partial \mathbf{U}}{\partial t} + \frac{\partial \mathbf{F}(\mathbf{U})}{\partial x} + \frac{\partial \mathbf{G}(\mathbf{U})}{\partial y} = \mathbf{S}(\mathbf{x}, \mathbf{y}, \mathbf{U}), \tag{1}$$

where the the expression for one layer is:

$$\mathbf{U} = \begin{pmatrix} h \\ hu \\ hv \end{pmatrix}, \qquad \mathbf{F} = \begin{pmatrix} hu \\ hu^2 + \frac{1}{2}gh^2 \\ huv \end{pmatrix},$$
$$\mathbf{G} = \begin{pmatrix} hv \\ huv \\ hv^2 + \frac{1}{2}gh^2 \end{pmatrix}, \quad \mathbf{S} = \begin{pmatrix} 0 \\ gh\left(\frac{\partial(z+h)}{\partial x} - \frac{\tau_x}{\rho}\right) \\ gh\left(\frac{\partial(z+h)}{\partial y} - \frac{\tau_y}{\rho}\right) \end{pmatrix}. \tag{2}$$

When describing a shallow water problem with two fluid layers, the formulation changes to:

$$\mathbf{U} = \begin{pmatrix} h_1 \\ h_1u_1 \\ h_1v_1 \\ h_2 \\ h_2u_2 \\ h_2v_2 \end{pmatrix}, \qquad \mathbf{F} = \begin{pmatrix} h_1u_1 \\ h_1u_1^2 + \frac{1}{2}gh_1^2 \\ h_1u_1v_1 \\ h_2u_2 \\ h_2u_2^2 + \frac{1}{2}gh_2^2 \\ h_2u_2v_2 \end{pmatrix},$$
$$\mathbf{G} = \begin{pmatrix} h_1v_1 \\ h_1u_1v_1 \\ h_1v_1^2 + \frac{1}{2}gh_1^2 \\ h_2v_2 \\ h_2u_2v_2 \\ h_2v_2^2 + \frac{1}{2}gh_2^2 \end{pmatrix}, \quad \mathbf{S} = \begin{pmatrix} 0 \\ gh_1\left(\frac{\partial(z_2+h_2)}{\partial x} - \frac{\tau_{x1}}{\rho_1}\right) \\ gh_1\left(\frac{\partial(z_2+h_2)}{\partial y} - \frac{\tau_{y1}}{\rho_1}\right) \\ 0 \\ gh_2\left(\frac{\partial z_2}{\partial x} - \frac{\tau_{x2}}{\rho_2} - r\frac{\partial h_1}{\partial x}\right) \\ gh_2\left(\frac{\partial z_2}{\partial y} - \frac{\tau_{y2}}{\rho_2} - r\frac{\partial h_1}{\partial y}\right) \end{pmatrix}, \tag{3}$$

where script 1 refers to the upper layer, and 2 to the lower layer (see figure 1), h is the depth of the fluid, u and v are the velocity component in the x and y directions, respectively, ρ is the density of the fluid, g the gravity acceleration value, r is the ratio of the densities (the terms τ/ρ are the energy slopes). To calculate these terms a Manning's relationship was used for layer 1, and a rheological model for layer 2.

The energy slope terms are calculated with, for the upper layer, the Manning's equation,and for the lower layer using the Turbulent, Coulomb and Yield rheological model (see [11]).

$$\frac{\tau_{x1}}{\rho_1} = S_{fx1} = \frac{n_1^2 u_1\sqrt{u_1^2+v_1^2}}{h_1^{4/3}}, \qquad \frac{\tau_{y1}}{\rho_1} = S_{fy1} = \frac{n_1^2 v_1\sqrt{u_1^2+v_1^2}}{h_1^{4/3}}, \tag{4}$$

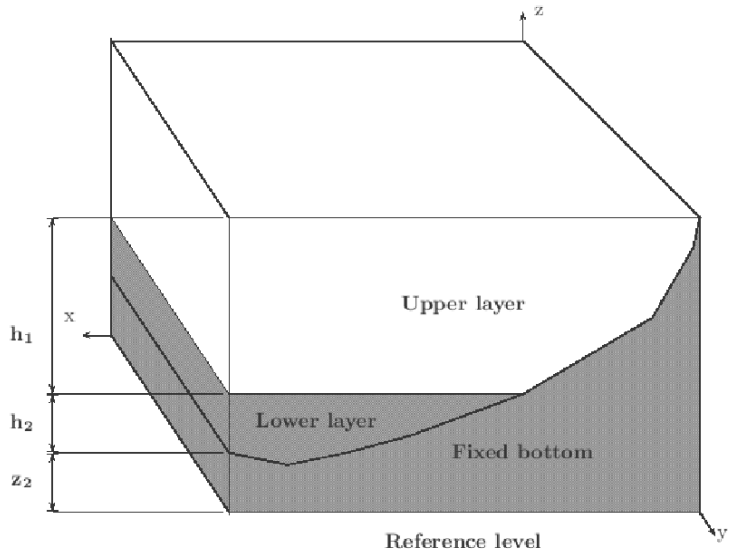

Figure 1.— Diagram of the two-layer model.

$$\begin{aligned}
\frac{\tau_{x2}}{\rho_2} &= S_{fx2} + \frac{\tau_i}{\rho_2 g h_2} = \frac{n_2^2 u_2 \sqrt{u_2^2 + v_2^2}}{h_2^{4/3}} + \frac{\tau_i}{\rho_2 g h_2}, \\
\frac{\tau_{y2}}{\rho_2} &= S_{fy2} + \frac{\tau_i}{\rho_2 g h_2} = \frac{n_2^2 v_2 \sqrt{u_2^2 + v_2^2}}{h_2^{4/3}} + \frac{\tau_i}{\rho_2 g h_2},
\end{aligned} \tag{5}$$

where n is the Manning's roughness coefficient, and τ_i is the shear stress, which must be overcome for the movement to start, and is estimated by:

$$\tau_i = \min\left(\tau_y, \rho_2 g h_2 \cos\alpha \tan\delta\right), \tag{6}$$

with α y δ the slope angle and the Coulomb friction angle, respectively. τ_y is the yield strength. All these parameters depend of the characteristic of the material.

A finite volume method to solve the system of equations was used. Reformulating system (1), we get

$$\frac{\partial \mathbf{U}}{\partial t} + \overrightarrow{\nabla}\mathbf{E}(\mathbf{U}) = \mathbf{S}(\mathbf{x}, \mathbf{y}, \mathbf{U}), \tag{7}$$

where the flux $\mathbf{E} = [\mathbf{F}, \mathbf{G}]$ is defined in order to highlight the conservative law structure of the system in the homogeneous case.

3 Numerical Model

In the two-dimensional approach presented in this work, the spatial domain of integration is covered by a set of cells, and a finite volume method is formulated where all the dependent variables of the system are represented as piecewise constant per cell. The

method used to solve the system of shallow water equations (1) will follow the previous works [8] and [7].

Integrating over the volume Ω the equation (7), leads to

$$\frac{\partial}{\partial t}\int_{\Omega}\mathbf{U}d\Omega+\int_{\Omega}(\overrightarrow{\nabla}\mathbf{E})d\Omega=\int_{\Omega}\mathbf{S}d\Omega. \tag{8}$$

Using the Gauss's theorem in the second term of the (8), gives

$$\frac{\partial}{\partial t}\int_{\Omega}\mathbf{U}d\Omega+\oint_{\delta\Omega}(\mathbf{E}\cdot\mathbf{n})d\Omega=\int_{\Omega}\mathbf{S}d\Omega. \tag{9}$$

The domain of integration is approximated by the sum over the grid cells.

$$\frac{\delta\mathbf{U_i}}{\delta t}A_i+\oint_{\partial\Omega}(\mathbf{E}\cdot\mathbf{n})dS=\int_{\Omega_i}\mathbf{S}d\Omega, \tag{10}$$

where A_i is the area of the cell Ω_i. The normal flux at the edge of the cells k is approximated by

$$\oint_{\partial\Omega}(\mathbf{E}\cdot\mathbf{n})dS\approx\sum_{k=1}^{NE}(\partial E_k\cdot n_k)s_k, \tag{11}$$

as an starting point for the derivation of the first order flux difference splitting technique, where k represents the index of the edge shared between cells Ω_i and Ω_m, the vector $\mathbf{n}_{i,k}$ is the unit outward normal in the cell Ω_i on edge k, l_k is the length of the edge k (see figure 2, where $i=R$ and $m=L$), $(\partial\mathbf{E}\cdot\mathbf{n})_{i,k}$ is the numerical flux difference across the cell edge, $\mathbf{E}_i$ and $\mathbf{E}_m$ are evaluated at cells m and i, and NE is the number of edges that define the cell.

The problem is then reduced to a one-dimensional Riemann problem projected onto the direction $\mathbf{n}_{i,k}$ at each cell edge. Roe [12] defined an approximated flux Jacobian, $\widetilde{\mathbf{J}}_\mathbf{n}$ for the Euler equations, and the approximate flux Jacobian for the coupled system shallow flow can be defined as

$$\partial\left(\mathbf{E}\cdot\mathbf{n}\right)_{i,k}=\widetilde{\mathbf{J}}_n\partial\mathbf{U}_{i,k}, \tag{12}$$

where

$$\widetilde{\mathbf{J}}_n=\begin{pmatrix}\widetilde{\mathbf{J}}_{n1} & \mathbf{0}\\ \mathbf{0} & \widetilde{\mathbf{J}}_{n2}\end{pmatrix}. \tag{13}$$

The elements of this matrix can expressed as follows:

$$\widetilde{\mathbf{J}}_{nj}=\begin{pmatrix}0 & n_x & n_y\\ (g\widetilde{h}_j-\widetilde{u}_j^2)n_x-\widetilde{u}_j\widetilde{v}_jn_y & \widetilde{v}_jn_y+2\widetilde{u}_jn_x & \widetilde{v}_jn_y\\ (g\widetilde{h}_j-\widetilde{v}_j^2)n_y-\widetilde{u}_j\widetilde{v}_jn_x & \widetilde{v}_jn_x & \widetilde{u}_jn_x+2\widetilde{v}_jn_y\end{pmatrix}, \tag{14}$$

where j is 1 for the upper-layer (clean water), and 2 for the lower-layer (mud flow).

The eigenvalues of the approximated Jacobian matrix are

$$\begin{array}{lll}\widetilde{\lambda}_k^1=\left(\widetilde{\mathbf{u}}_\mathbf{1}\cdot\mathbf{n}+\widetilde{c}_1\right)_k, & \widetilde{\lambda}_k^2=\left(\widetilde{\mathbf{u}}_\mathbf{1}\cdot\mathbf{n}\right)_k, & \widetilde{\lambda}_k^3=\left(\widetilde{\mathbf{u}}_\mathbf{1}\cdot\mathbf{n}-\widetilde{c}_1\right)_k,\\ \widetilde{\lambda}_k^4=\left(\widetilde{\mathbf{u}}_\mathbf{2}\cdot\mathbf{n}+\widetilde{c}_2\right)_k, & \widetilde{\lambda}_k^5=\left(\widetilde{\mathbf{u}}_\mathbf{2}\cdot\mathbf{n}\right)_k, & \widetilde{\lambda}_k^6=\left(\widetilde{\mathbf{u}}_\mathbf{2}\cdot\mathbf{n}-\widetilde{c}_2\right)_k,\end{array} \tag{15}$$

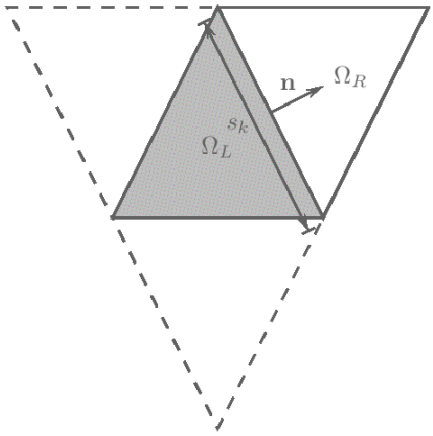

Figure 2.— Diagram of the triangle cell.

and the corresponding eigenvectors are

$$\widetilde{\mathbf{e}}^{\mathbf{1}} = \begin{pmatrix} 1 \\ \widetilde{u}_1 + \widetilde{c}_1 n_x \\ \widetilde{v}_1 + \widetilde{c}_1 n_y \\ 0 \\ 0 \\ 0 \end{pmatrix}, \quad \widetilde{\mathbf{e}}^{\mathbf{2}} = \begin{pmatrix} 0 \\ -\widetilde{c}_1 n_y \\ \widetilde{c}_1 n_x \\ 0 \\ 0 \\ 0 \end{pmatrix}, \quad \widetilde{\mathbf{e}}^{\mathbf{3}} = \begin{pmatrix} 1 \\ \widetilde{u}_1 - \widetilde{c}_1 n_x \\ \widetilde{v}_1 - \widetilde{c}_1 n_y \\ 0 \\ 0 \\ 0 \end{pmatrix},$$

$$\widetilde{\mathbf{e}}^{\mathbf{4}} = \begin{pmatrix} 0 \\ 0 \\ 0 \\ 1 \\ \widetilde{u}_2 + \widetilde{c}_2 n_x \\ \widetilde{v}_2 + \widetilde{c}_2 n_y \end{pmatrix}, \quad \widetilde{\mathbf{e}}^{\mathbf{5}} = \begin{pmatrix} 0 \\ 0 \\ 0 \\ 0 \\ -\widetilde{c}_2 n_y \\ \widetilde{c}_2 n_x \end{pmatrix}, \quad \widetilde{\mathbf{e}}^{\mathbf{6}} = \begin{pmatrix} 0 \\ 0 \\ 0 \\ 1 \\ \widetilde{u}_2 - \widetilde{c}_2 n_x \\ \widetilde{v}_2 - \widetilde{c}_2 n_y \end{pmatrix}. \tag{16}$$

Roe's average approximation is used, thus,

$$\widetilde{u}_j = \frac{u_{Rj}\sqrt{h_{Rj}} + u_{Lj}\sqrt{h_{Lj}}}{\sqrt{h_{Rj}} + \sqrt{h_{Lj}}}, \quad \widetilde{v}_j = \frac{v_{Rj}\sqrt{h_{Rj}} + v_{Lj}\sqrt{h_{Lj}}}{\sqrt{h_{Rj}} + \sqrt{h_{Lj}}}, \quad \widetilde{c}_j = \sqrt{g\frac{h_{Rj} + h_{Lj}}{2}}. \tag{17}$$

Following a flux difference procedure, the difference in vector $\mathbf{U}$ across the edge is projected onto the matrix eigenvectors basis as

$$\delta\mathbf{U} = \sum_{m=1}^{N\lambda} (\alpha\widetilde{\mathbf{e}})_k^m, \tag{18}$$

where the expression of coefficients α_k are

$$\begin{aligned}
\alpha_k^{1,3} &= \frac{\delta h_{1,k}}{2} \pm \frac{1}{2\widetilde{c}_{1,k}} \left(\delta \mathbf{q}_{1,k} - \widetilde{\mathbf{u}}_{1,k}\delta h_{1,k}\right) \cdot \mathbf{n}, \quad \alpha_k^2 = \frac{1}{2\widetilde{c}_{1,k}} \left(\delta \mathbf{q}_{1,k} - \widetilde{\mathbf{u}}_{1,k}\right) \cdot \mathbf{n}_T, \\
\alpha_k^{4,6} &= \frac{\delta h_{2,k}}{2} \pm \frac{1}{2\widetilde{c}_{2,k}} \left(\delta \mathbf{q}_{2,k} - \widetilde{\mathbf{u}}_{2,k}\delta h_{2,k}\right) \cdot \mathbf{n}, \quad \alpha_k^5 = \frac{1}{2\widetilde{c}_{2,k}} \left(\delta \mathbf{q}_{2,k} - \widetilde{\mathbf{u}}_{2,k}\right) \cdot \mathbf{n}_T,
\end{aligned} \tag{19}$$

and $\mathbf{q}_j = (q_{xj}, q_{yj})$ (j is 1 for upper layer, and 2 for the lower layer), and $n_T = (-n_y, n_x)$ is the tangential vector to the edge.

The $\delta\mathbf{E} \cdot \mathbf{n_k}$ contributions at a cell edge k can be written as

$$\delta\mathbf{E} \cdot \mathbf{n_k} = \sum_{k=1}^{NE} \sum_{m=1}^{N\lambda} (\widetilde{\lambda}^m \alpha^m \widetilde{\mathbf{e}}^{\mathbf{m}})_k l_k. \tag{20}$$

The bed slope and the rheological source terms have been discretized, according to [13], in an upwind form in order to ensure the best discrete balance with the flux terms at least in steady state. At every edge k of every cell Ω_i the source term participates with the in-going contributions built as before:

$$\mathbf{U_i^*} = \mathbf{U_i^n} - \sum_{k=1}^{NE} \sum_{m=1}^{N\lambda} ((\widetilde{\lambda}^m \alpha^m - \beta^{m-}) \widetilde{\mathbf{e}}^{\mathbf{m}})_i^n \frac{s_k}{A_i} \Delta t, \tag{21}$$

such that coefficients β are defined as

$$\begin{aligned}
\beta^1 &= -\frac{\widetilde{c}_1}{2}\delta z_1, \quad \beta^2 = 0, \\
\beta^3 &= \frac{\widetilde{c}_1}{2}\delta z_1, \qquad \beta^4 = -\frac{\widetilde{c}_2}{2}\left(\delta z_2 + \frac{\tau_i d_n}{\rho_2 g \widetilde{h}_2} + r\delta h_1\right), \\
\beta^5 &= 0, \qquad\qquad \beta^6 = -\frac{\widetilde{c}_2}{2}\left(\delta z_2 + \frac{\tau_i d_n}{\rho_2 g \widetilde{h}_2} + r\delta h_1\right),
\end{aligned} \tag{22}$$

where d_n is the distance between cell centroids projected onto the $\mathbf{n}$ vector, and $\widetilde{h}_2 = \frac{1}{2}(h_{2R} + h_{2L})$, is depth average between neighboring cells.

To avoid oscillations in the solution, the following condition must be fulfilled

$$(\mathbf{hu})_i^{n+1} = \begin{cases} \geq 0 & \text{if} \quad (\mathbf{hu})_i^n > 0 \\ \\ \leq 0 & \text{if} \quad (\mathbf{hu})_i^n < 0 \end{cases} \qquad (\mathbf{hv})_i^{n+1} = \begin{cases} \geq 0 & \text{if} \quad (\mathbf{hv})_i^n > 0 \\ \\ \leq 0 & \text{if} \quad (\mathbf{hv})_i^n < 0 \end{cases} \tag{23}$$

In order to avoid that the rheological term would be unable to change the sign of the discharges, the following conditions are enforced over the unit discharge function **hu**:

$$(\mathbf{hu})_i^{n+1} = (\mathbf{hu})_i^n - \left(\frac{h_i g \tau^* d_n l_k}{A_i}\right)_i^n \Delta t = (\mathbf{hu})_i^n \left(1 - \frac{g\tau^* d_n l_k}{\mathbf{u}_i^n} \Delta t\right), \tag{24}$$

where τ^* is the second term of the equation (5).

To satisfy condition (23), the following condition over the time step is proposed:

$$\Delta t = CFL \quad \min \left\{ \frac{A_{\min,k}}{\max\left[|\widetilde{\lambda}_k^m|\right] l_k}, \frac{|\widetilde{\mathbf{u}}| A_{\min,k}}{g\tau d_n l_k} \right\}_{k=1,Nedge} \tag{25}$$

The first term of (25) represents the time step condition according of the numerical model (more details in [8]), and the second one, is the time step restriction to satisfy (23) to prevent change in the direction of the discharges.

4 Applications

4.1 Test Cases

In order to evaluate the behavior of the proposed model, a series of numerical test cases haven been analyzed. Twelve different test cases were invented, but only three of them are presented in this work. The computation domain for all cases is 2000 m and 20 m, and the Manning's roughness coefficient is 0.2 $s/m^{1/3}$. Two different conditions were analyst for each case, two liquid layers and liquid and mud layers.

In the case of two liquid layers, the ratio of densities used was $r = 0.98$. For liquid and mud layers, the value of r was 0.56, the yield strength 2300 Pa and the $\delta = 10$. All computational cases were simulated with different grid refinement, with no significant differences in the results.

4.1.1 Test Case 1

In this case, a dam break of the lower layer was analysed. Figure 3a and figure 4a show the initial condition for two liquid layers and liquid and mud layers, respectively. The initial level of the upper layer was 50 m and for the lower layer 30.5 m, in both cases.

Figure 3 shows the results for the test case 1 for liquids layers. As it can be seen in the results, the model behaves according which expected. The equilibrium condition obtained with the model, for the liquid layers test case, is horizontal (see figure 3d).

On the other hand, for the liquid and mud layers, the equilibrium condition for the upper layer was horizontal, that is the equilibrium condition of liquid (see figure 4d).

4.1.2 Test Case 2

In this case, the symmetry in the final solution is evaluated. The initial conditions are shown in the figures 5a and 6a for the two liquid layers, and liquid and mud layers, respectively. They show a huge column of material of layer 2 in the center of the domain. The height of the column of mud is the 50 m and the level of the water is 30.5 m. Besides, to evaluate the discretizetation of the bed slope term, the level bottom elevation

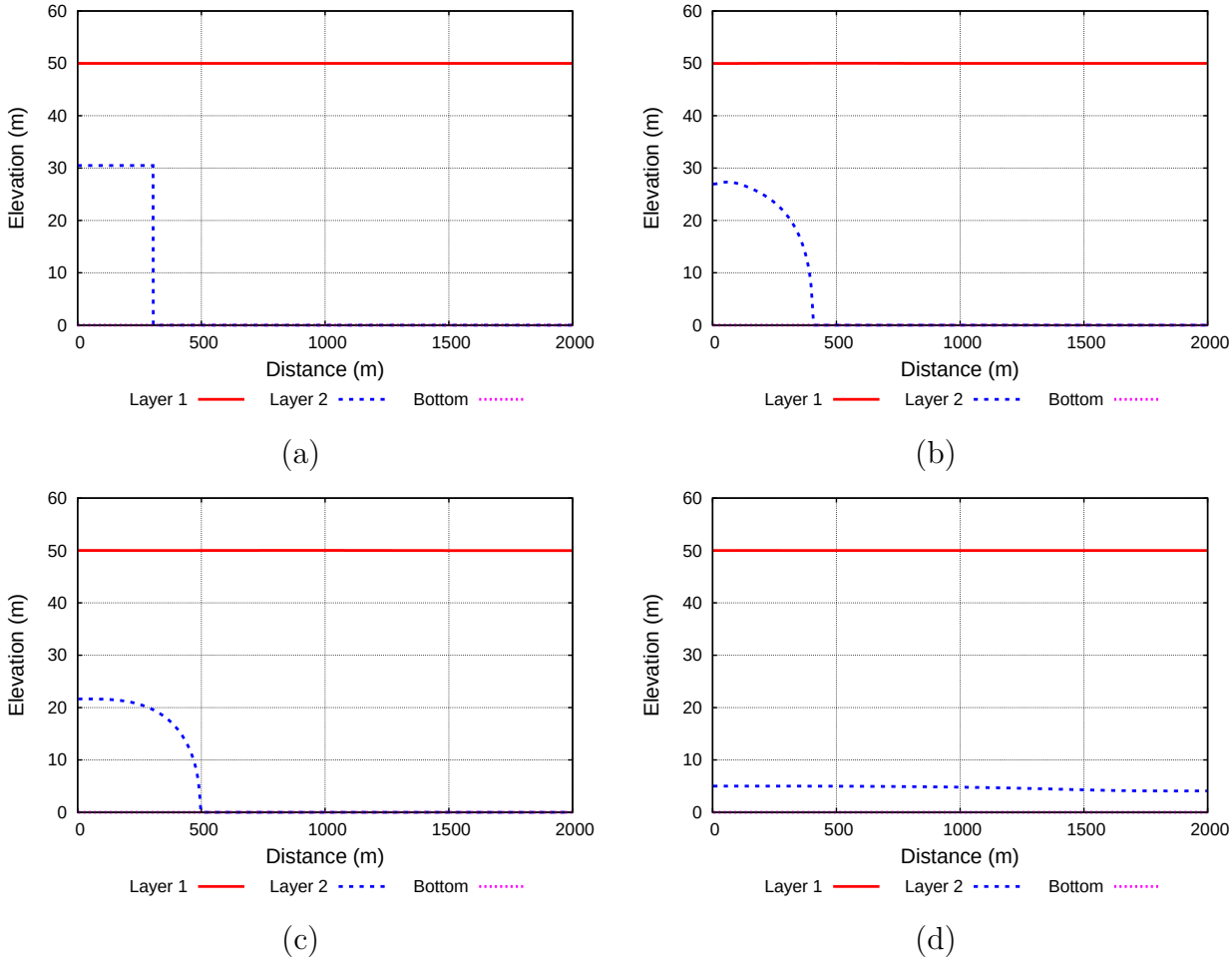

Figure 3.— Results for the Test Case 1 for two liquid layers, (a) initial condition, (b) 200 s, (c) 500 s, and (d) equilibrium condition.

is variable. The aim of these examples was to evaluate the symmetry in the results during the simulation.

Plots 5b, and 5c show the results at 200 s, and 500 s, respectively. These plots show that the symmetry in the results is satisfied for this case. For the liquid and mud layers (see plots 6b and 6c) this symmetry is satisfied as well.

The equilibrium condition for the two liquid layers is shown in the plot 5d. The graphics shows again that the obtained levels for both layers is horizontal. For the liquid and mud layers, the equilibrium condition is displayed in figure 6d. Besides, for the upper layer, the obtained level is horizontal and solution is symmetry.

4.1.3 Test Case 3

In this case, the lightest layer was located in the middle of the domain (layer 1), and at the edges of the domain, there are two columns of layer 2. As well as in the previous example, the idea of this case is to evaluate the symmetry in the solution during the simulation. In this case, the level of the lightest layer is 30.5 m height and 50 m for the

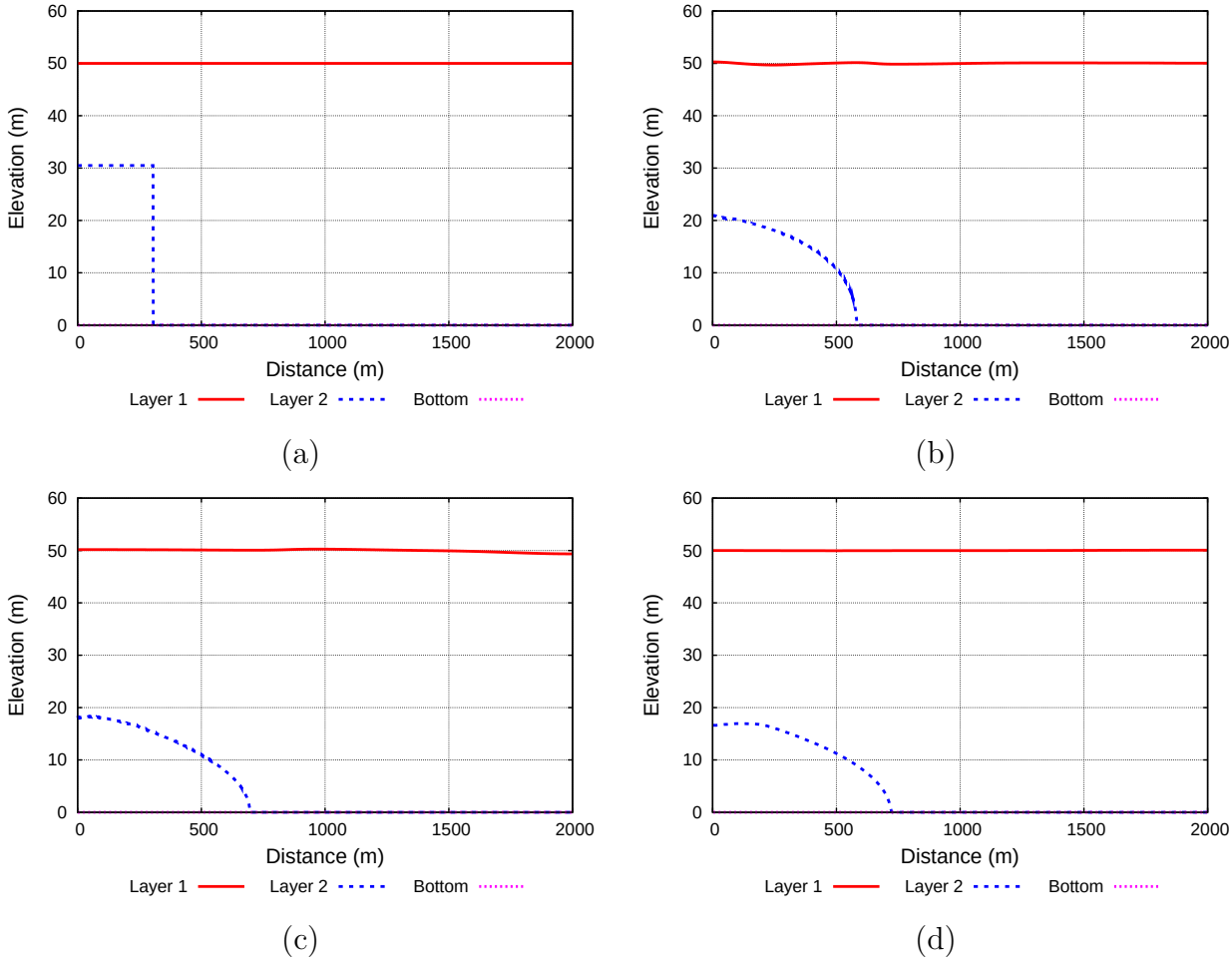

Figure 4.— Results for the Test Case 1 for liquid and mud layers, (a) initial condition, (b) 200 s, (c) 500 s, and (d) equilibrium condition.

other layer (layer 2), and the bottom elevation is variable, and has the same shape of the test case 2.

Figure **??** show the initial condition, the results at 200 s, 500 s and the equilibrium condition for the two liquid layers. As shown there, the results are symmetric during the simulation (see figure **??**b, and **??**c). Figure **??**d shows that the equilibrium condition the level of both layers is horizontal.

On the other hand, in figures 8 display the initial, results at 200 s, 500 s, and equilibrium conditions for the liquid and mud layers. The obtained results for this case show the symmetry in the solution during the simulation as well, and the equilibrium level for the upper layer is horizontal.

4.2 Santa Liestra Dam Project

The presented in the previous section will be applied to a case characterized by irregular cross section and realistic dimensions. The problem consists of the evaluation of the consequences of the potential catastrophic displacement of an important volume of solid

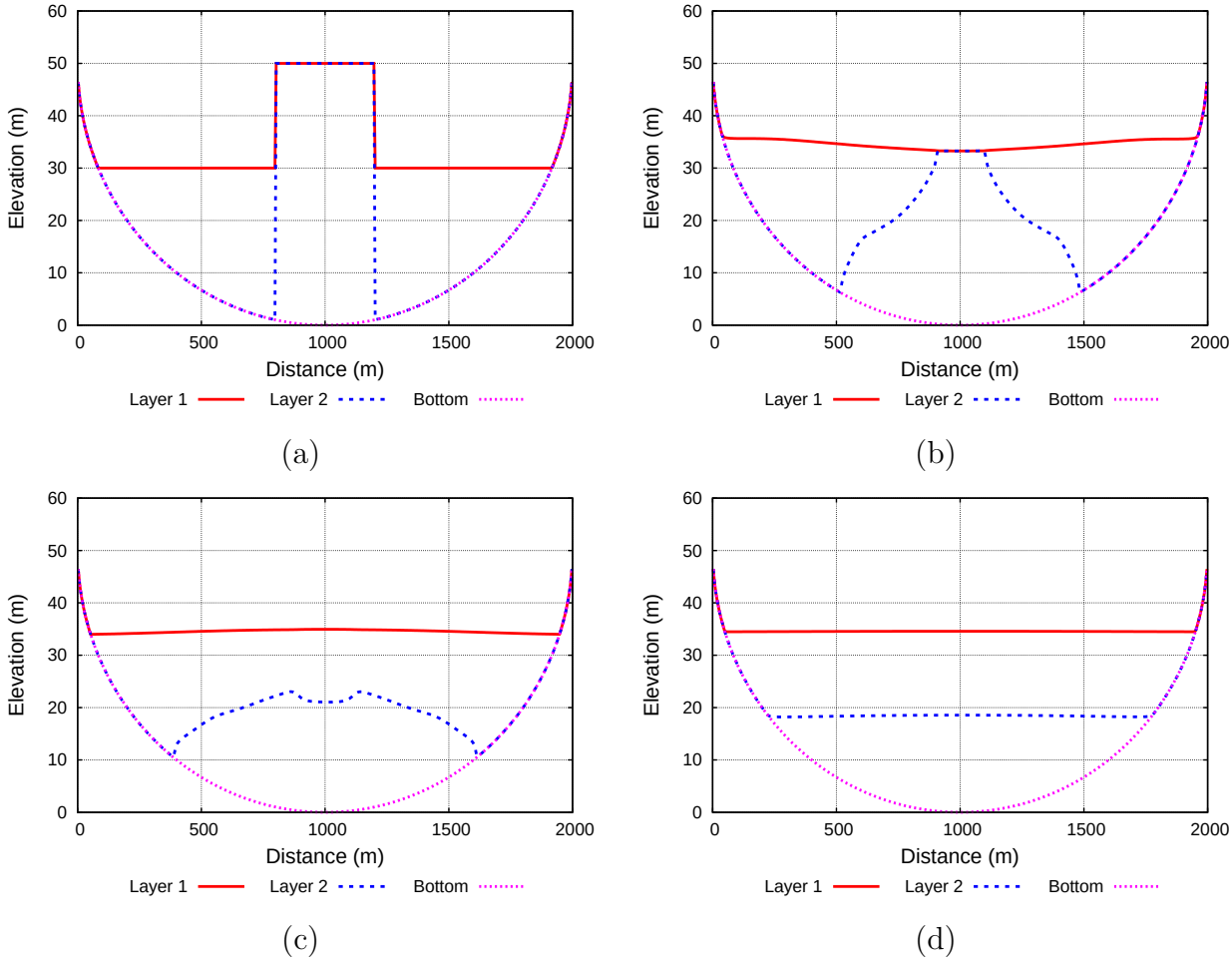

Figure 5.— Results for the Test Case 2 for two liquid layers, (a) initial condition, (b) 200 s, (c) 500 s, and (d) equilibrium condition.

material into the dam project Santa Liestra reservoir, on the Esera river in the Spanish Pyrenees. The construction of the reservoir at that location is intended to regulate 81.9 Hm^3, at the upper part of the river. In 2000, CEDEX made an internal report [3] and obtained some useful geological data [1]. Figure 9, shows the topographic location of the reservoir. The maximum envisaged water level is 642 m (full reservoir) and the location of the potential sliding area at the left bank of the Esera river. The volume of the materials involved is around 20 Hm^3 according to the geological prospections. Besides, the kind of materials and their fractured and weathered state, and the fact that the lower land would become saturated when filling the reservoir contribute to the possibility of a sudden failure. The present work, however, does not focus on the conditions under which the slide could be triggered. This study starts from the hypothesis that the slide takes place and is motivated by the consequences of the impact over the stored water in the reservoir. The maximum risk scenario follows the hypothesis made in previous studies [3]. The figure 10d shows the condition at time 400 s, at this time the reservoir will be separated in two water bodies. For this reason, the area at the end of the reservoir will

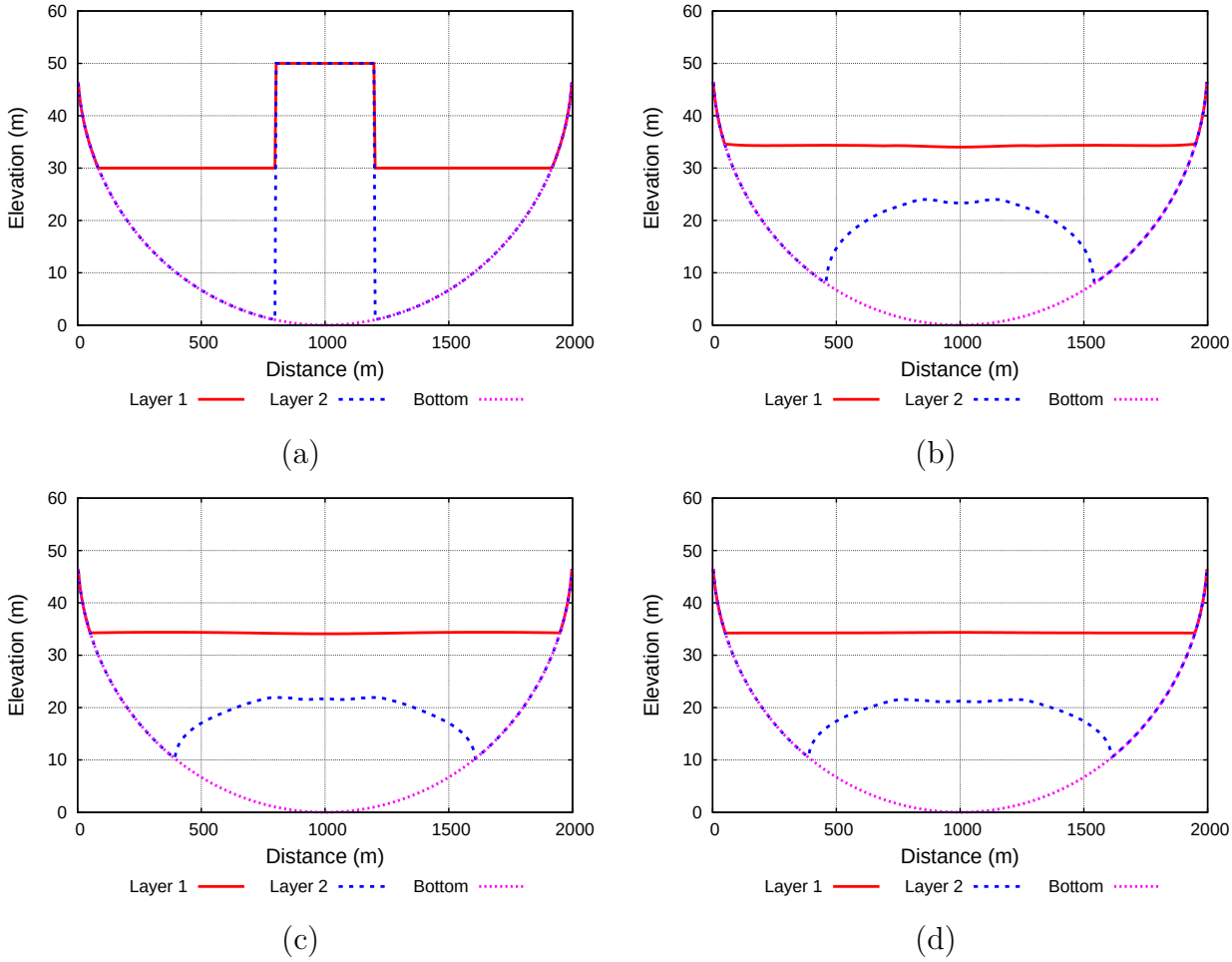

Figure 6.— Results for the Test Case 2 for liquid and mud layers, (a) initial condition, (b) 200 s, (c) 500 s, and (d) equilibrium condition.

be flooded. In order to have an idea of the volume of the material, the figures 10 show the form of bottom level and water surface level longitudinal longitudinal profiles along the river axis. In figure 10b shows of the falling material at 50 s after the beginning of landslide. At that time, almost landslide material has fallen into the reservoir.

The parameters of the rheological model have been modified, in order to analysis the sensitivity of the model. The different values used were chosen for the different soil characteristics. The frictional angle was tested with values between 10 and 30 degrees, and the yield strength between 1000 and 3000 Pa, with no significant differences in the final results. The results presented for this paper in figure 10 were for 10 degrees for the angle and 2300 Pa for the yield strength.

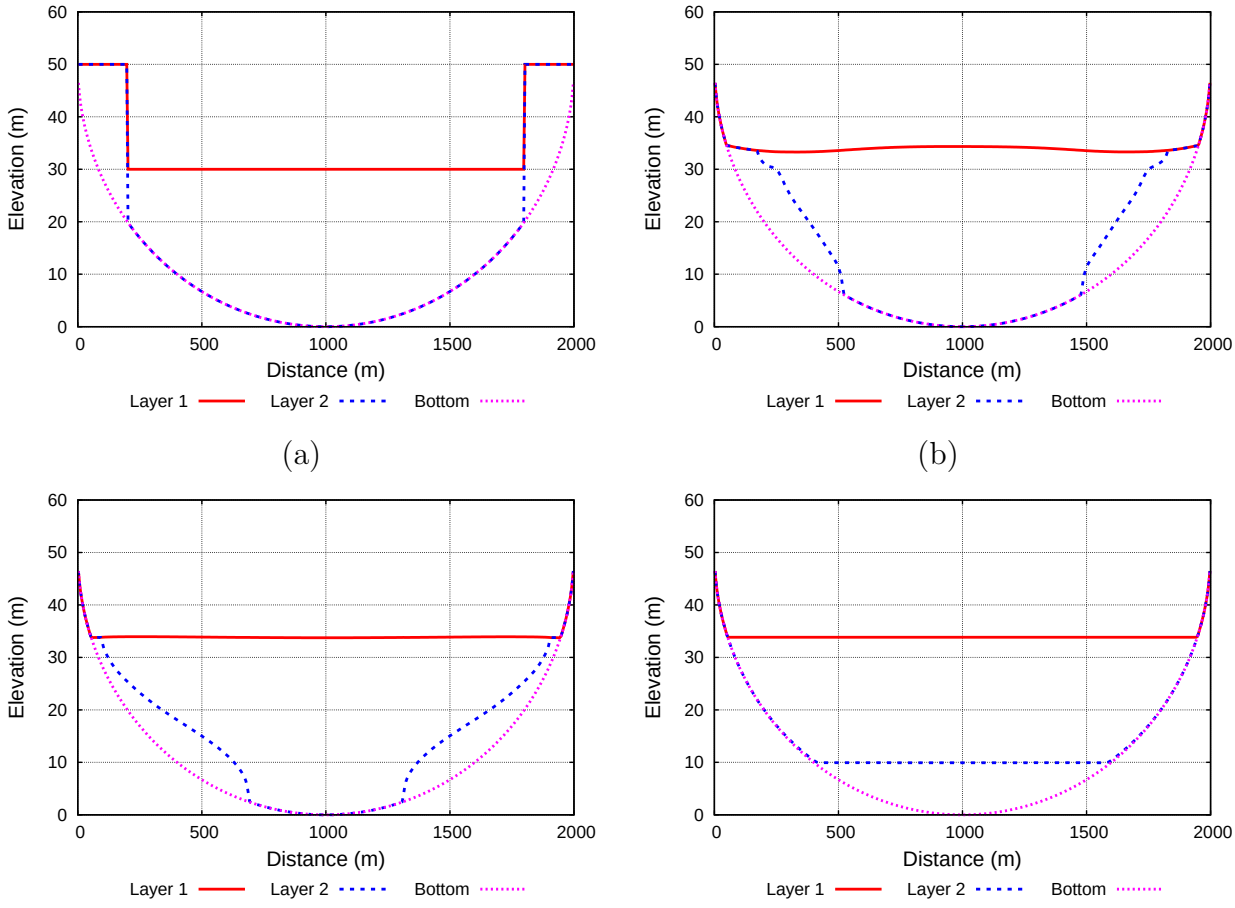

Figure 7.— Results for the Test Case 3 for two liquid layers, (a) initial condition, (b) 200 s, (c) 500 s, and (d) equilibrium condition.
labelcase31

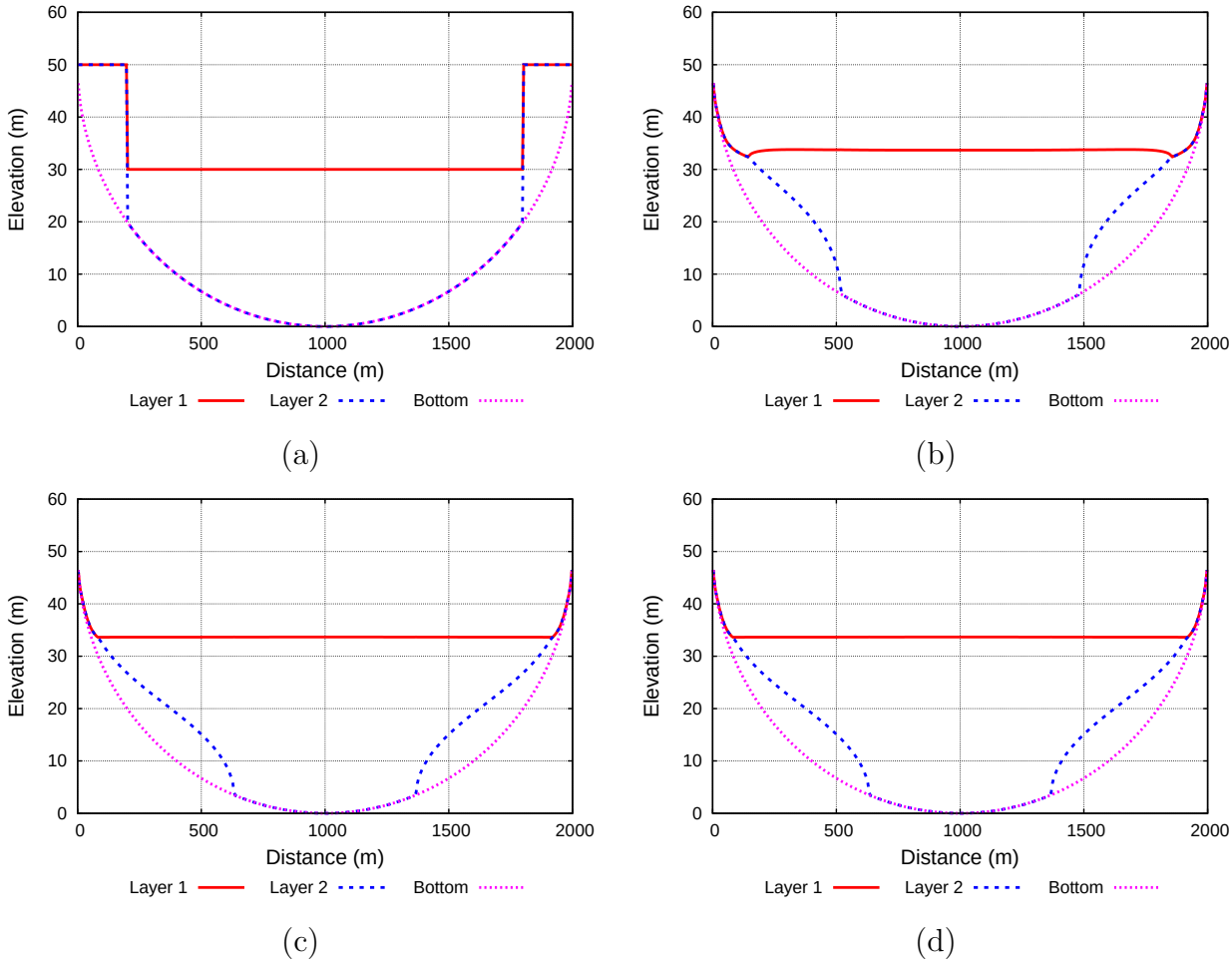

Figure 8.— Results for the Test Case 3 for liquid and mud layers, (a) initial condition, (b) 200 s, (c) 500 s, and (d) equilibrium condition.

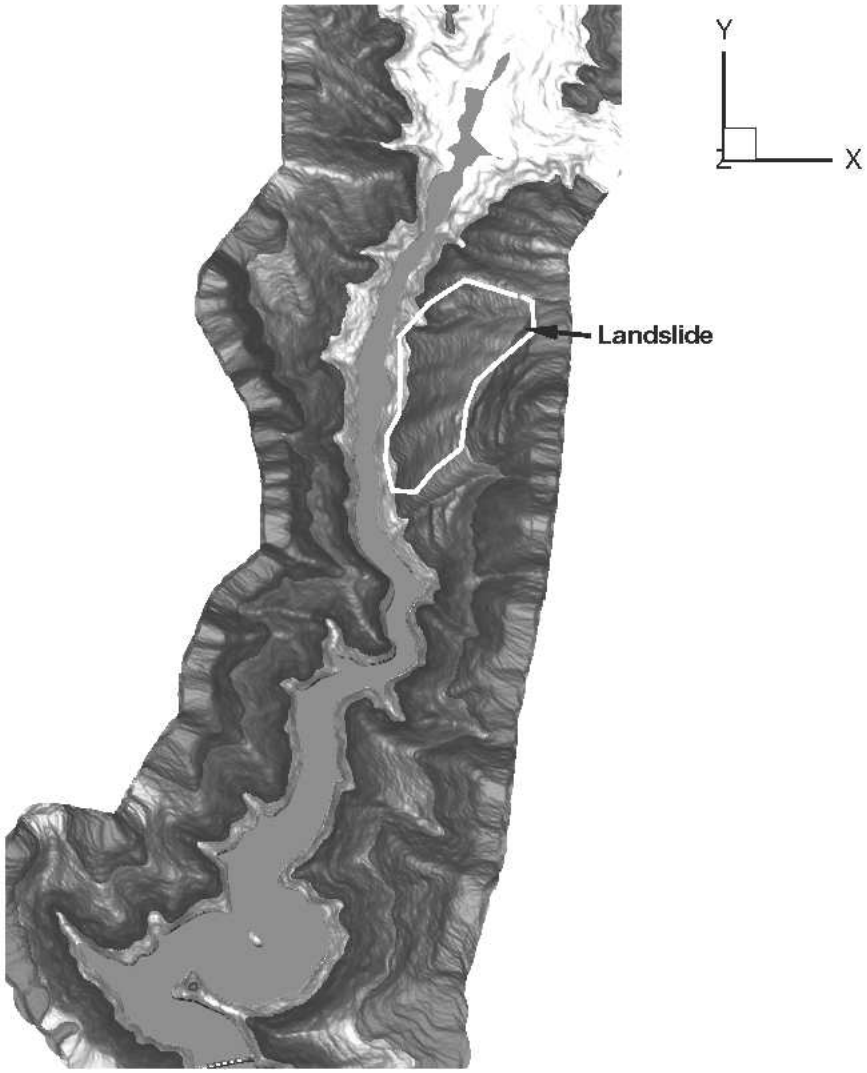

Figure 9.— View plant of the Santa Liestra dam project.

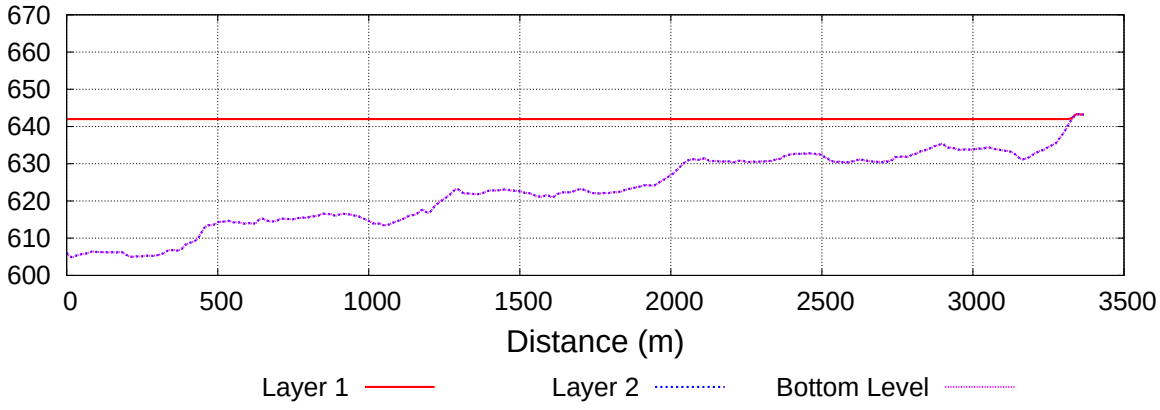

(a)

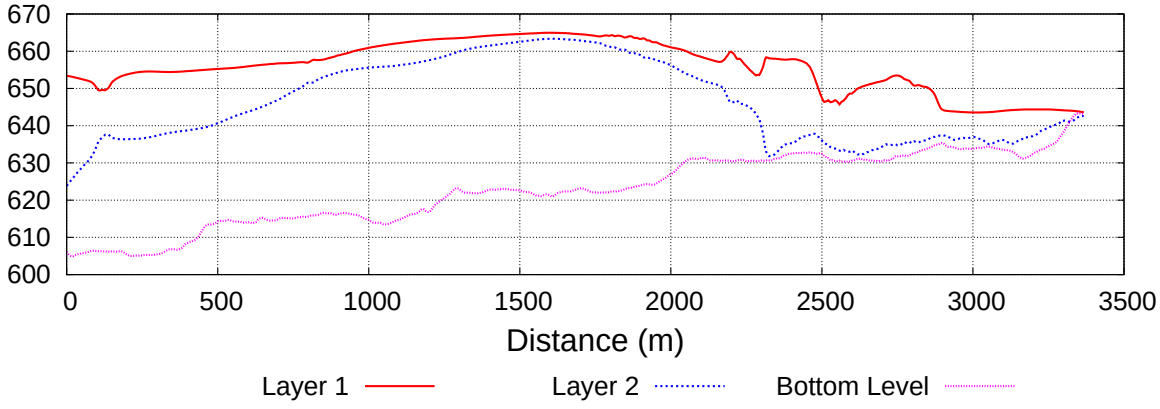

(b)

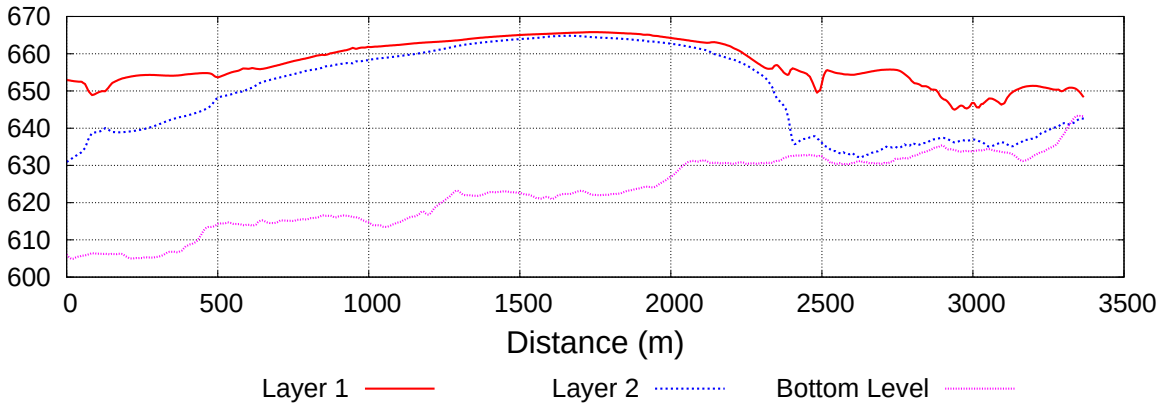

(c)

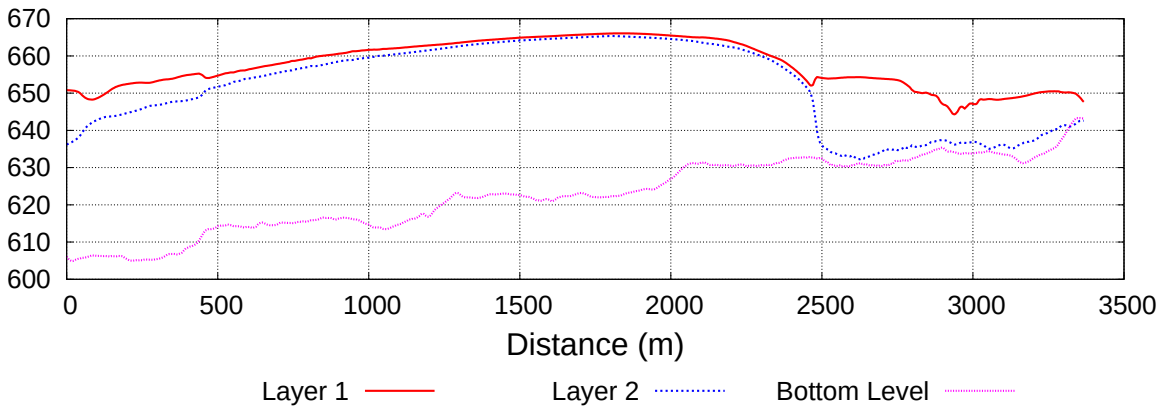

(d)

Figure 10.— Longitudinal section of the Esera river at (a) 0 s, (b) 50 s, (c) 100 s, and (d) 200 s.

5 Conclusions

The proposed model has been presented as a tool to simulate landslide movements and their interaction with shallow water bodies.

From the numerical point of view, it can be concluded that the scheme used is appropriate for this kind of problem. Besides, the mass conservation analysis gave errors on the order of 10^{-5} %. All the cases (except of the Santa Liestra dam project) were simulated using a several degrees of grid refinement. Numerical solutions become grid independent.

The sensitive analysis showed that the rheological model used does not present significant changes in the results with different values of the parameters.

Although further validation of this model is required, the proposed methodology can be considered a valuable starting point. This study shows the need of the experimental data on this field.

Future work envisaged to incorporate more rheological relationships, in order to increase the application range of the model is envisaged.

References

[1] A. M. Casas Sainz. Evolución de varmints y riesgos geológicos en el Esera medio (tramo Santa Liestra-Morillo de Liena). *Informe técnico (in Spanish). Departamento de Ciencias de la Tierra, Universidad de Zaragoza*, 1997.

[2] L. Cea, A. Ferreiro, M. E. Váquez-Cendón and J. Puertas. An experimental and numerical analysis of solitary waves generated by bed and boundary movements. *International Journal of Numerical Methods in Fluids* **46**, 793–813, 2004.

[3] CEDEX. Asesoramiento geotécnico para el estudio de la cerrada de la presa y la evaluación de las condiciones de estabilidad de las zonas denominadas P. K. 56 y P. K. 52 del embalse de Santa Liestra. Apéndice 4: Modelización de los deslizamientos de laderas en el P. K. 56b y propagación de la onda estraordinaria en el embalse. *Informe técnico (in Spanish)*, 2000.

[4] R. Fernandes de Carvalho, J. S. Antunes do Carmo and A. Pestana. Waves caused by landslides into reservoirs and their impacts on dams. *International Junior Researcher and Engineer Workshop ob Hydraulic Structures* 2006.

[5] H. M. Fritz, W. H. Hager and H. E. Minor. Near field characteristics of landslide generated impulse waves. *Journal of Waterway, Port, Coastal, and Ocean Engineering* 287–300, 2004.

[6] P. Y. Julien and Y. Lan. Rheology of hyperconcentrations. *Journal of Hydraulic Engineering* **117**(3), 346–353, 1991.

[7] J. Murillo, J. Burguete, P. Brufau, and P. García-Navarro. Coupling between shallow water and solute flow equations: analysis and management of source terms in 2D. *International Journal of Numerical Methods in Fluids* **49**, 267–299, 2005.

[8] J. Murillo, P. García-Navarro, J. Burguete and P. Brufau. A conservative 2D model of inundation flow with solute transport over dry bed. *International Journal of Numerical Methods in Fluids* **52**, 1059–1092, 2005.

[9] P. Lynett and P. Liu. A numerical study of the run-up generated by three-dimensional landslides. *Journal of Geophysical Research-Oceans* **110**(C3), 2005.

[10] G. Pérez, P. García-Navarro and M. E. Váquez-Cendón. One-dimensional model of shallow water surface waves generated by landslides. *Journal of Hydraulic Engineering* **132**(2), 2006.

[11] D. Rickenmann, D. Laigle, B. W. MacArdell and J. Hübl. Comparison of 2D debris-flow simulation models with field events. *Computational Geosciences* **10**, 241–264, 2006.

[12] P. L. Roe. Discrete models for the numerical analysis of time dependent multidimensional gas dynamics *Journal of Computational Physics* **63**, 458–476, 1986.

[13] M. E. Vázquez-Cendón. Improved treatment of source terms in upwind schemes for the shallow water equations in channels with irregular geometry. *International Journal of Computational Physics* **148** 497–526, 1999.